applied sciences

MDPI

Article

Effect of Cyclic Load Amplitude on the Evolving Characteristics of Accumulative Deformation in Subgrade Bed

Gang Liu [1,2,3], Mingzhi Zhao [1,2,*], Qiang Luo [3,4] and Hongyu Jia [4]

1 School of Civil Engineering, Architecture and Environment, Xihua University, Chengdu 610039, China; 0120130047@mail.xhu.edu.cn
2 Institute of Geotechnical Engineering, Xihua University, Chengdu 610039, China
3 MOE Key Laboratory of High-Speed Railway Engineering, Southwest Jiaotong University, Chengdu 610031, China; Lqrock@home.swjtu.edu.cn
4 School of Civil Engineering, Southwest Jiaotong University, Chengdu 610031, China; Hongyu_swjtu@swjtu.edu.cn
* Correspondence: 1220180013@mail.xhu.edu.cn

Received: 20 February 2019; Accepted: 2 April 2019; Published: 5 April 2019

Abstract: To investigate the evolving characteristics of plastic deformation for the angular gravels that are used to construct subgrade bed, a laboratory model test is performed with cyclic load applying. Vertical deformation is measured in real time by displacement transducers and further modified to analyze the plastic behavior of model fillings. It can be found that vertical plastic deformation shows quite different developing patterns under the effect of different cyclic amplitudes for a given model. A power function is adopted to describe the relationship between deformation rate and loading times. By analyzing the value of the power exponent and the corresponding developing features of plastic deformation rate, model filling status can be classified into four different zones, i.e., rapid stabilization, tardy stabilization, tardy failure, and rapid failure. Such a classification reveals different developing patterns of plastic deformation and satisfies the design of subgrade bed for ballasted and unballasted railway.

Keywords: subgrade bed; angular gravel; accumulative deformation; rapid stabilization; tardy stabilization; tardy failure; rapid failure

1. Introduction

Due to rapid operating trains, high-speed railway raises more rigorous requirements for smoothness and stability of rail track. To ensure the service performance of rail track, it is critical to make effective control of cumulative deformation that occurs at substructures (subgrade bed and subsoil) and ground. The subgrade bed, which refers to the uppermost structure that directly bears the cyclic load from train and rail track, generally have a thickness ranging from 2.0 m to 3.0 m [1–3]. Since subsoil and ground are mainly composed of fine-grained soils, greater post-construction deformation is likely to occur at these positions compared with subgrade bed. Therefore, the cumulative deformation of ballast layer and subgrade bed should be more strictly controlled to make space for the deformation at other positions.

To investigate the deformation property of ballast layer and subgrade bed, various kinds of research means, such as laboratory test, filed instrumentation, discrete element method, and finite difference method, have been adopted by researchers to study the mechanical behavior of coarse-grained fillings. A three-dimensional discrete element model was established by Zhang et al. [4] to simulate the realistic ballast particle shapes. With such a model, it can be concluded that load

frequency has a significant effect on ballast permanent deformation when it is beyond 15 Hz. Moreover, both laboratory test and numerical analysis are performed by Ngo et al. [5] to study the deformation and degradation of ballast when subjected to cyclic loading. A numerical model, which can be adopted to predict the deformation response of rail track, was developed. Since many theoretical models about track settlement and ballast deformation were developed in the previous literature, Dahlberg [6] makes a summary to demonstrate the advantages and disadvantages of the models when they are used to predict the long-term deformation of substructure. Although many tests and models have already been developed to evaluate the deformation produced at rail substructures, most of them mainly focus on the deformation at ballast layer or the whole system.

Currently, two kinds of technical measurements, improving both the quality and compaction degree of fillings, are adopted to restrain the cumulative deformation that occurs at subgrade bed. In Japan, surface layer of subgrade bed is constructed layer-by-layer with asphalt concrete and graded gravel (or blast furnace slag) so that it can suffer the dynamic train load [1]. Meanwhile, it is stipulated in Germany that the fillings in surface layer of subgrade bed should be dominated by coarse-grained soils. Moreover, compaction degree is restricted to be not less than 100% for surface layer and 97% for bottom layer [3]. In China, well graded angular gravel is recommended to fill surface layer, while round gravel, pebble, gravelly sand, and soil should be adopted to build the bottom layer of subgrade bed. The thickness of subgrade bed is set to be 3.0 m for the ballasted track and 2.7 m for the unballasted one [2]. Although the design criteria have already been described in detail in the codes of some countries, evolvement characteristic for cumulative deformation under cyclic load is not sufficiently considered in these design codes. In particular, ballast bed, which underlies the rail track in the ballasted railway, has a better adaptive capacity for deformation compared to the concrete slab in the unballasted one. Furthermore, new railway ballast can be replenished to ballast bed to raise track to the original location for the ballasted railway once relatively large plastic deformation has occurred. It is remarkable that the ballasted track is much easier to maintain and preserve than the unballasted one. Thus, the requirements of cumulative deformation should be different for the ballasted and unballasted railway, which is worthy of consideration in the design process.

To restrict the cumulative deformation to a reasonable magnitude, predicting and evaluating the definite value or evolvement tendency of plastic deformation is needed in the first place. Two kinds of approaches are adopted to analyze the characteristics of cumulative deformation under cyclic load. The first is to develop numerical analysis model to predict the development law of cumulative deformation with increasing loading times [7–13]. This method aims at evaluating the final definite value of the plastic deformation. The other approach focuses on the evolutive states of plastic deformation [14–17]. Deformation rate is plotted against loading times under different levels of cyclic load so that different plastic stages can be categorized in terms of tracing pattern. With the characteristics of deformation rate clearly classified, the tendency of plastic deformation can be evaluated. As mentioned above, the requirements of restricting the cumulative deformation of subgrade bed is extremely rigid. Especially, the post-construction deformation has been limited to millimeter-scale for the whole substructure and ground for high-speed railway. It seems to be quite difficult to use the first method to predict the definite value due to the extremely small plastic deformation compared with the height of substructure. Therefore, the second approach, which discusses the characteristics of deformation status against loading times, is more popular to predict plastic deformability.

In the previous literature, several classifications of plastic deformation tendency have been put forward on a basis of characteristics of deformation rate. Heath [18] and Cai & Cao [19] have performed triaxial cyclic loading tests on London clay and Chengdu clay, respectively, and obtained cumulative plastic deformation curve plotted against loading times. They classified the curves into generative pattern and degenerative one, which represents ever-increasing and converging plastic deformation respectively. Obviously, only two states, the steady state and the collapse one, are identified in their framework. Werkmeister [15] has conducted 100 groups of triaxial tests at different stress levels on

graded gravel and sandy gravel. Based on the evolving law of cumulative plastic deformation rate, the state of plastic strain has been divided into three categories, i.e., plastic shakedown, plastic creep, and exacerbation. Plastic shakedown implies that plastic strain of fillings tends to a certain value under some cyclic loading level and plastic deformation rate gradually decreased to zero. Meanwhile, exacerbation represents that the deformation rate is continuously increased under cyclic loading, and soil structure is rapidly collapsed with just a few loading times. It should be noted that there is a transitional state termed as plastic creep. In this state, cumulative deformation rate decreases in initial loading stage, and then levels off with the increasing loading times. At the same time, plastic strain is almost linearly increased with loading times, which finally leads to the soil structure broken down. Minassian [20] also classified the evolving tendency of plastic deformation under cyclic loading into three groups, i.e., stable state, critical state, and unstable state. However, stability of critical state is ambiguous and need further discussion. In addition, Hoff et al. [21] concluded that only elastic strain exists on the condition of small magnitude of cyclic loading. With the increasing loading level, plastic deformation emerges but finally converges to a stable state. When cyclic loading remains relatively large, plastic strain is accumulated and finally makes soil structure break down.

Summarily, two ultimate states, which are the stable one that only elastic strain can be observed at low cyclic loading level and the collapsed one that cumulative deformation continuously develops at high loading amplitude, exactly exist. When stress level stays moderate, whether the corresponding critical state develops towards stabilization or collapse remains disputable. However, it is obvious that both stabilization and collapse can be differentiated into the rapid one and tardy one. This grouping conception is of great significance for the design of subgrade bed in terms of cumulative deformation. Despite the difference of limiting value of cumulative deformation between ballasted and unballasted track in high-speed railway, both types of rail tracks should finally tend to stabilization under billions of cyclic loading times. In this study, a subgrade bed model test is performed to investigate the development of cumulative deformation. A power function model has been established to describe the evolvement characteristics of plastic strain rate against cyclic loading times. The power exponent is chosen as the critical parameter to identify the different evolving states. With threshold values of power exponent determined on a basis of the laboratory model test, four plastic evolving states can be classified quantitatively. The conclusions will provide guidance for the design of subgrade bed for both ballasted and unballasted track.

2. Model Test Scheme

2.1. Model. Configuration

A subgrade model is constructed to investigate the plastic behavior of subgrade fillings. A round of brick walls are firstly built in the forms that four corners are not overlapped with each other, so that a cube space is developed with the brick walls as boundaries. The cube space is 100 centimeters (cm) in height with an intersecting square whose side length is 70 cm. The actual height of subgrade fillings is 90 cm. The sandbags are piled up around the brick walls to create nonrigid boundaries for the model. The detail of model configuration is shown in Figure 1.

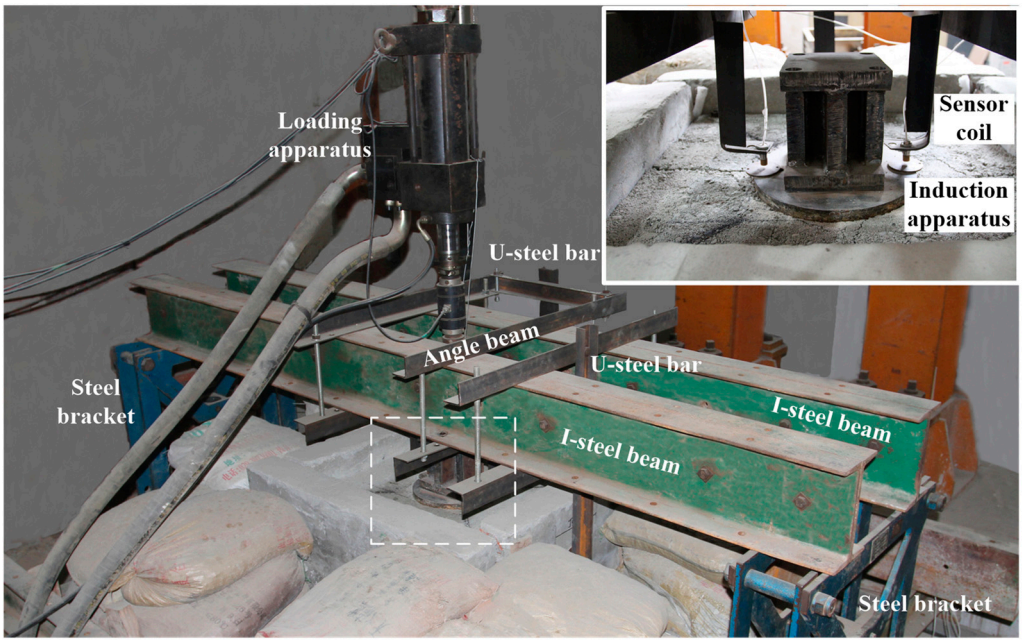

Figure 1. Model configuration.

The steel beams and bars are set to provide locations to place displacement transducers. Two steel brackets are set up on both sides of the model to support the I-steel beams, which are used to hold angle steel bars. The sensor coils of eddy current displacement transducers, which provide information for vertical displacement of the model surface, are attached to the angle steels. In addition to the sensor coils, two U-steel bars are also dependent on the angel steel to provide locations for the transducers to measure the horizontal displacement of the filling model under cyclic loading. Above the model is the loading apparatus which provides cyclic loading, as shown in Figure 1.

2.2. Displacement Transducer Layout

A bearing plate with a diameter of 30 cm is located in the center of the filling model. Since cyclic loading head is not long enough to reach the bearing plate, a dynamic load transfer device is placed on the central position of the bearing plate. Adjacent to the load transfer device are two eddy current vertical displacement transducers. These two displacement transducers are used to measure the vertical deformation. The eddy current displacement transducers are mainly composed of induction apparatus distributed on the bearing plate and sensor coil hanging below the angle steel. Once the bearing plate is descending under cyclic load, there is a variation of magnetic flux under the effect of sensor coil. Furthermore, inductive eddy will be produced on the surface of induction apparatus, which is an indicator of vertical displacement of the model surface.

Six horizontal displacement transducers are placed on the surrounding brick walls. In detail, three are installed on the south wall, and another three are on the east wall. These six transducers are divided into three groups to measure the horizontal displacement of model fillings 10 cm, 30 cm, and 50 cm below model surface. The horizontal displacement transducers have the same working mechanism as the vertical ones. The sensor coils keep still upon the U-steel bars, which are depended on angle steel bars and finally attached to the steel brackets on the ground. When horizontal displacement occurs, the induction apparatus on the brick wall will move outward, leading to the variation of eddy current. At last, the transducers will give the exact value about the horizontal displacement. The layout of displacement transducers is shown in Figure 2. All the transducers are marked from No. 1 to No. 8 to distinguish from each other.

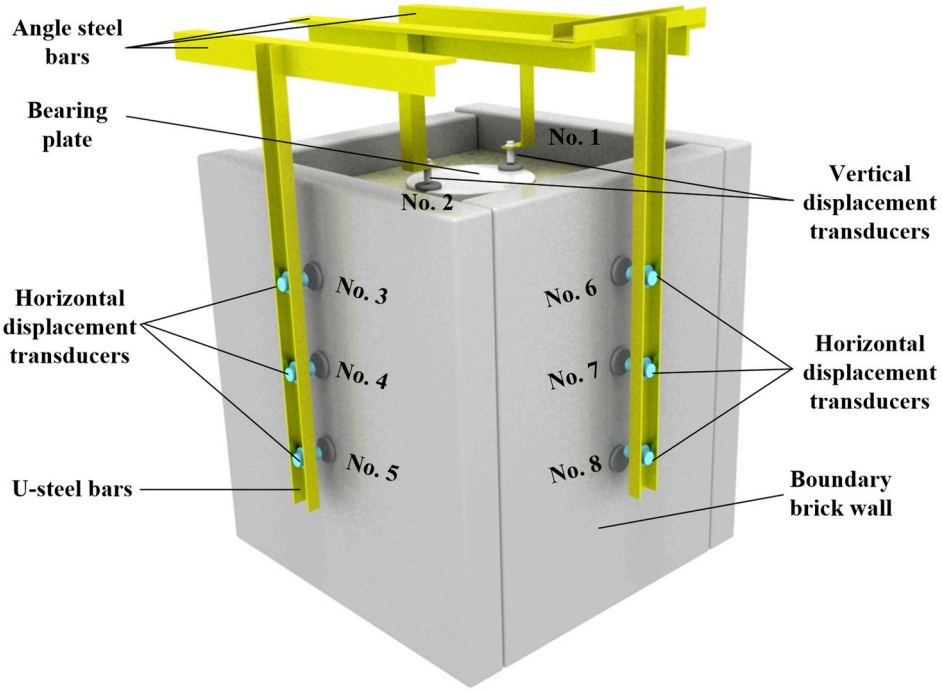

Figure 2. Displacement transducers layout.

2.3. Test. Model. Filling

The fillings are mainly composed of angular graded gravels. Sieve test is carefully performed to obtain the characteristics of particle size distribution. The grading curve is shown in Figure 3. All of the filling particles can pass the 40 mm sieve, indicating that the maximum particle size is smaller than 40 mm. More than 50% particles have a size smaller than 10 mm. Only 6.82% particles could pass the 0.075 mm sieve. Furthermore, nonuniform coefficient of the fillings is 67 and curvature coefficient is 4.67. Therefore, the fillings can be distinguished as fine angular pebbles with some clayey soil. Furthermore, since the top layer of subgrade bed suffers cyclic train load and climate changes directly, its size grading is strictly regulated in Chinese code and should locate in the scope shown by the upper and lower limited grading lines in Figure 3. It is remarkable that the graded gravel adopted in this study have the size grading characteristics that satisfy such a requirement.

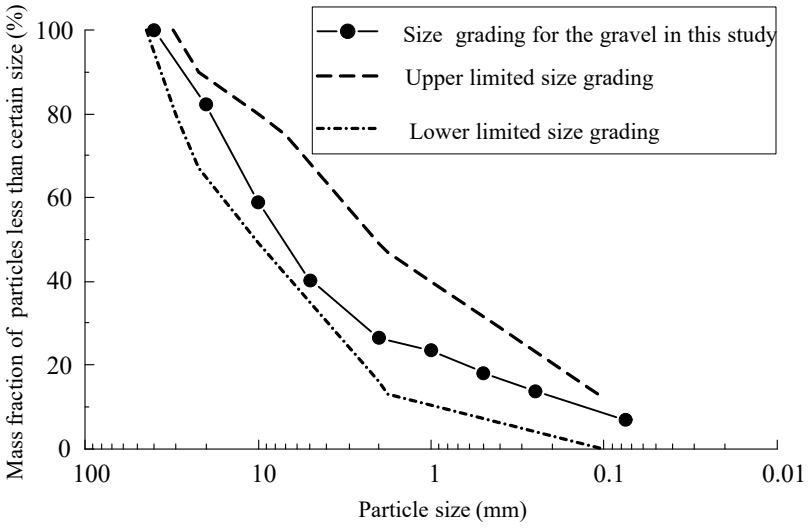

Figure 3. Particle size distribution of model filling.

After this, standard heavy compaction test is carried out for the fillings to obtain the maximum dry density and optimum moisture content. The compaction work per unit volume applied in the standard heavy compaction test is 2684.9 kJ/m^3. With analysis of the compaction test data, the maximum dry density $\rho_{d\max}$ is approximately equal to 2.40 g/cm^3, while the optimum moisture content is nearly 5.3%.

The fillings are prepared to have the optimum moisture content to fill the test model. The model is filled by four layers in a layer-by-layer manner. The thicknesses of the four layers are 20 cm, 20 cm, 25 cm, and 25 cm respectively from bottom to top. Three models with different compaction degrees are constructed as a comparison with each other. The compaction degree K is defined by the following equation:

$$K = \frac{\rho_d}{\rho_{d\max}} \tag{1}$$

where ρ_d is dry density of the filling model. The compaction degree of these three models and the corresponding filling mass for each structural layer are listed in Table 1. After each layer is filled into the model, it is compacted by artificially ramming to finish the construction.

Table 1. Compaction degree for each model and filling mass for each layer.

Model No.	Compaction Degree	Layer	Thickness (cm)	Filling Mass (kg)
Model 1	0.9	Lower two layers	20	222
		Upper two layers	25	278
Model 2	0.95	Lower two layers	20	235
		Upper two layers	25	293
Model 3	1.0	Lower two layers	20	247
		Upper two layers	25	309

As soon as construction is finished, ground coefficient K_{30} for each model is precisely measured by load settlement test. It should be noted that ground coefficient K_{30} refers to the ratio of dead load corresponding to fiducial settlement to fiducial settlement. Generally, fiducial settlement is set as 1.25 mm. K_{30} is widely adopted in high-speed railway construction in Japan and China. The relationship between settlement and load level is measured for these three models, as shown in Figure 4. According to the test data, ground coefficient K_{30} can be calculated as 136 MPa/m, 224 MPa/m, and 373 MPa/m for the models with compaction degree of 0.9, 0.95, and 1.0 respectively. It is remarkable that the model with higher compaction degree is inclined to have a larger value of K_{30}.

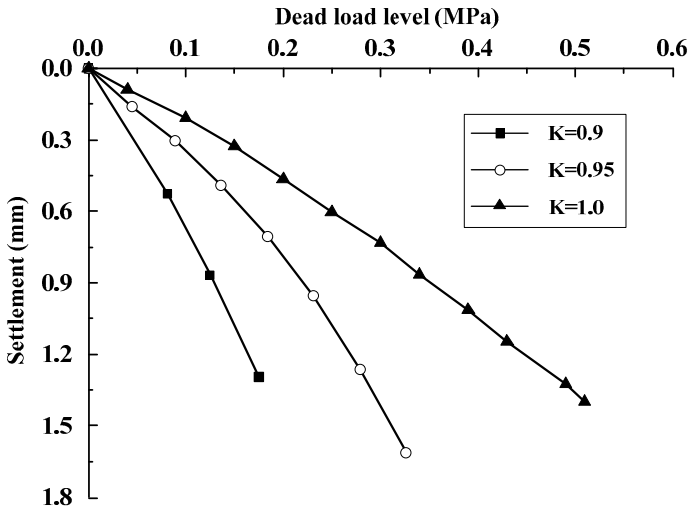

Figure 4. The relationship between settlement and dead load level in K_{30} test.

2.4. Loading Program

Hydraulic-driven loading test system is adopted in this model test to provide cyclic loading. Two kinds of loads, dead load P_s and cyclic load P_d, are applied in the loading process. It is worth noting that dead load P_s is composed of three components: mass of load transfer device P_{s1}, mass of loading head P_{s2}, and the third part that is imposed by the loading test system P_{s3}. In initial stage, the load transfer device is located on the bearing plate and only P_{s1} is imposed on the plate. Then the loading head slides gradually down towards the load transfer device under the effect of its own gravity on the condition that the power of loading system still stays off. Meanwhile, mass of the loading head P_{s2}, together with P_{s1}, is imposed on the bearing plate jointly. To ensure the loading head keeps contact with the load transfer device from beginning to end in the loading process, the third part of dead load P_{s3} is imposed by the loading system with the power turning on. At last, different levels of cyclic loads are applied on the test model to investigate the characteristics of plastic deformation under cyclic loading.

The first load level in cyclic loading process is 50 kPa. Next, the cyclic loading is increased by 50 kPa to 400 kPa, and then continuously raises up by 100 kPa till 700 kPa, in the following steps: 50 kPa, 100 kPa, 150 kPa, 200 kPa, 250 kPa, 300 kPa, 350 kPa, 400 kPa, 500 kPa, 600 kPa, 700 kPa. It is noted that ultimate bearing capacity for the filling models with different compaction coefficient K are quite different. Therefore, the maximum cyclic loads applied on the three models are 300 kPa, 500 kPa, and 700 kPa respectively. The amplitude of cyclic loads and loading times for these three models are shown in Table 2.

Table 2. Amplitude of cyclic loads and loading times for three models.

Model No.	Compaction Degree	Loading Level	Loading Amplitude (kPa)	Loading Times (Thousand Cycles)
M1	0.90	1	50	100
		2	100	100
		3	150	100
		4	200	100
		5	250	50
		6	300	10
M2	0.95	1	50	100
		2	100	100
		3	150	100
		4	200	100
		5	250	100
		6	300	100
		7	350	100
		8	400	100
		9	500	20
M3	1.0	1	50	100
		2	100	100
		3	150	100
		4	200	100
		5	250	100
		6	300	100
		7	350	100
		8	400	100
		9	500	100
		10	600	100
		11	700	35

The actual load frequency suffered by subgrade bed is not a constant value. It is difficult to simulate continuous change of various load frequencies in a model test. Therefore, a load frequency of

5 Hz is adopted. At the beginning of cyclic loading stage, the frequency of cyclic loads could not be too large in case that overlarge impulsive force will influence the stability of model structure. Therefore, loading frequency gradually increases from 1 Hz to 5 Hz at each cyclic loading level. Initially, cyclic load is imposed with 1 Hz loading frequency for the first 1000 loading times. Then, loading frequency increases step-by-step to 2 Hz, 3 Hz, and 4 Hz for the second, third, and fourth 1000 loading times. Finally, the cyclic load stays stable at 5 Hz for the remaining 96,000 times. In total, the cyclic loading is applied for 100,000 times at each loading level. When a certain level of cyclic loading is over, only dead loads are imposed on the bearing plate till the next level of cyclic load is coming. The cyclic loading program is shown in detail in Figure 5.

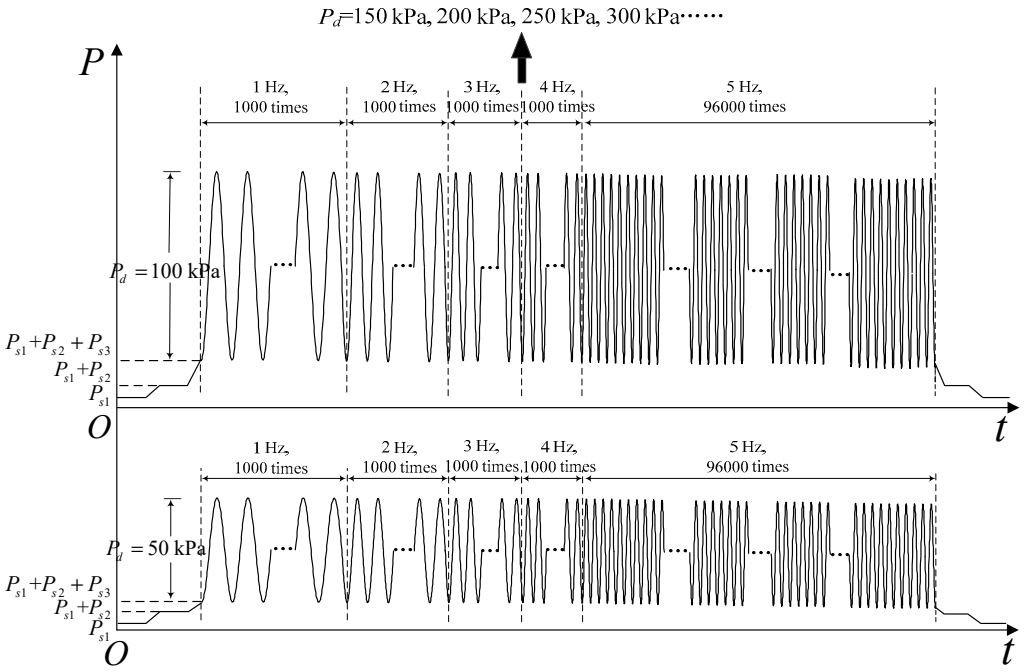

Figure 5. Cyclic loading program.

3. Response of Plastic Deformation in Model Test

3.1. Vertical Deformation Under Cyclic Loading

The vertical deformation is precisely measured by the vertical displacement transducers located on the model surface in real time. When P_d = 100 kPa, the displacement of Model 3 measured by the No.1 vertical transducer is shown in Figure 6. Figure 6a depicts the evolvement characteristics of measured deformation in the entire cyclic loading process. Figure 6b, which shows the deformation curve from 545 s to 590 s in the initial stage, is obtained from the deformation curve in the dotted box of Figure 6a and enlarged along the x direction. The deformation development demonstrates sine shaped curve in loading and unloading cycles. It is clearly indicated that both elastic and plastic deformations occur in the loading process, while only elastic deformation is recoverable during the unloading stage. In other words, a certain level of plastic deformation is sustained and developed during each loading and unloading cycle. Therefore, plastic displacement is continuously accumulated under the effect of cyclic loading. However, the growth rate of accumulated plastic deformation is gradually decreased with elapsed time (loading times) increasing under 100 kPa cyclic amplitude, which finally leads to the stable plastic displacement when loading times reach a relatively high level, as shown in Figure 6a.

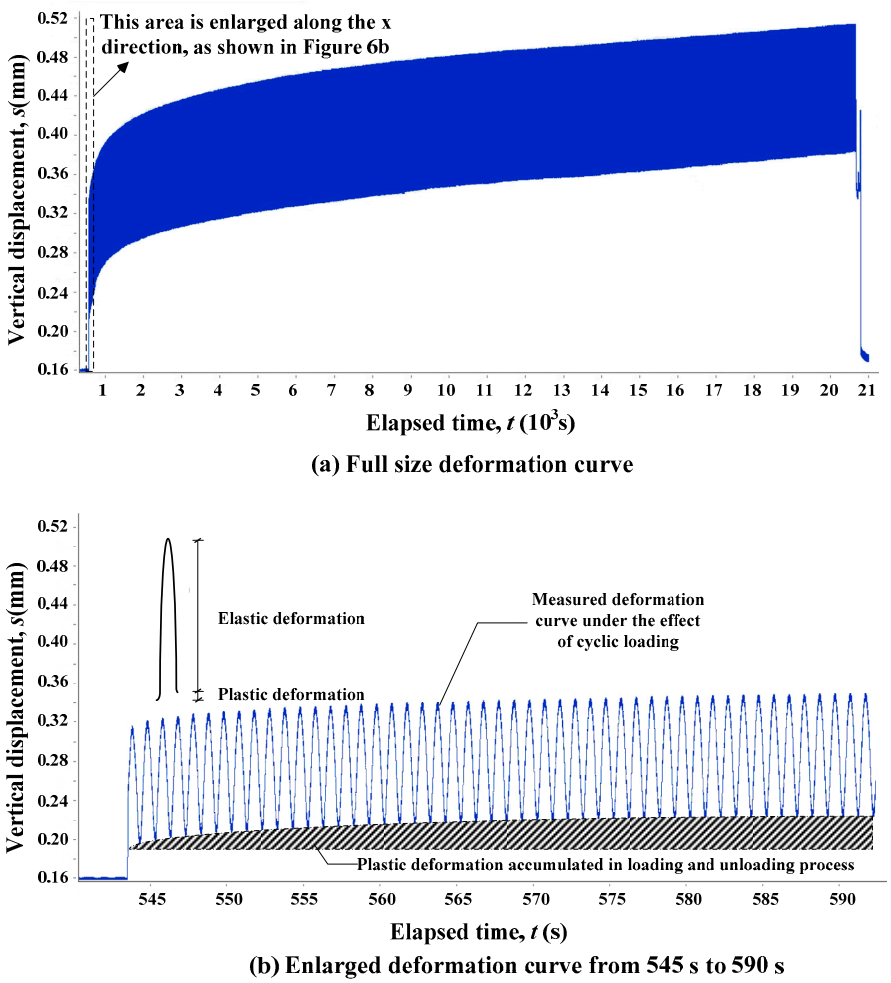

Figure 6. Vertical displacement for Model 3 (K = 1.0) under 100 kPa cyclic loading level.

When cyclic loading level P_d ranges from 100 kPa to 700 kPa, the vertical deformation curves for Model 3 (K = 1.0) are measured by No.1 vertical transducer, as shown in Figure 7. Figure 7a–d show the curves corresponding to the condition of P_d = 100 kPa, P_d = 300 kPa, P_d = 500 kPa, and P_d = 700 kPa respectively. When P_d = 100 kPa and P_d = 300 kPa, vertical plastic deformations are finally increased quite slowly as the loading times arrive at a relatively large magnitude. Moreover, the deformations at 100,000 loading times when P_d equals to 100 kPa and 300 kPa are close to 0.50 mm and 0.85 mm, respectively. Obviously, as the amplitude of P_d increases, vertical plastic deformation is obviously improved. On the condition of P_d = 500 kPa and P_d = 700 kPa, vertical plastic deformation develops continuously with the increasing loading times. When P_d = 700 kPa, the vertical deformation rate of the filling model even increases with loading times, which undoubtedly leads to the soil structure collapse rapidly at the initial stage of cyclic loading process. Summarily, the development of plastic deformation tends to converge when amplitude of cyclic loading is relatively small for a given model with a certain compaction degree. As the cyclic loading amplitude increases, the converging deformation is also steadily improved. When the loading amplitude reaches to some extent, the tendency of the plastic displacement gradually become diverging and deformation will abidingly develop with the ever-increasing loading times. If the amplitude of cyclic load keeps growing, plastic deformation will develop at an amazing speed and model structure will break down rapidly.

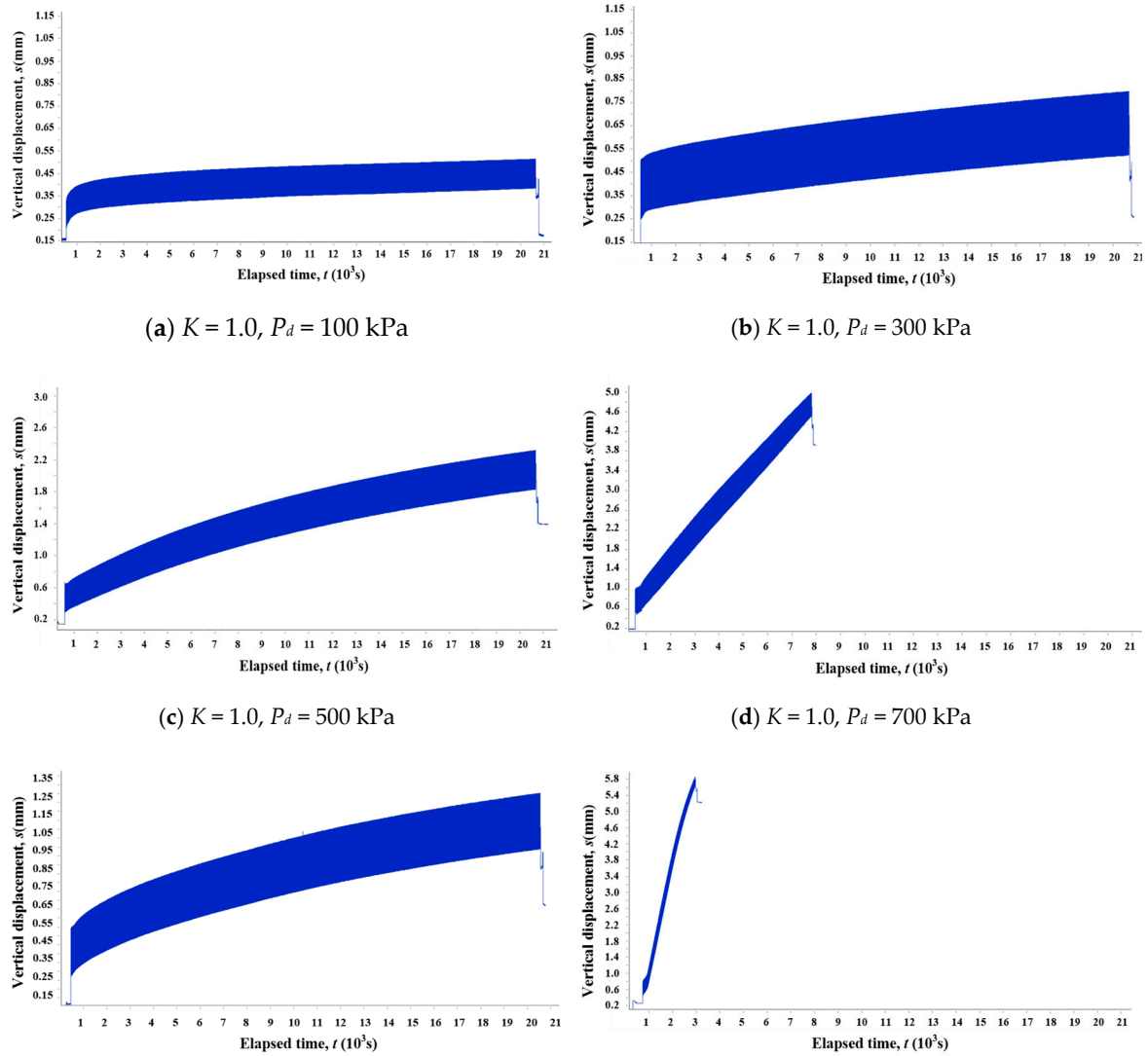

(**a**) K = 1.0, P_d = 100 kPa (**b**) K = 1.0, P_d = 300 kPa

(**c**) K = 1.0, P_d = 500 kPa (**d**) K = 1.0, P_d = 700 kPa

(**e**) K = 0.95, P_d = 300 kPa (**f**) K = 0.90, P_d = 300 kPa

Figure 7. Vertical displacement for the three models under cyclic loading.

Except for amplitude of cyclic loading, compaction degree K of the model filling may be another factor that can obviously influence the development characteristics of plastic deformation under dynamic load. Take Figure 7b, Figure 7e, and Figure 7f to make a comparison, plastic deformation is precisely measured when amplitude of cyclic loading equals to 300 kPa for the three models. The difference is that compaction degrees for these three models are 1.0, 0.95, and 0.9 respectively. Obviously, under the effect of the same cyclic loading amplitude, plastic deformation of Model 3 (K = 1.0) tends to converge towards 0.85 mm, while deformations of Model 2 (K = 0.95) and Model 1 (K = 0.9) remarkably show divergency. Furthermore, the evolutive rate of plastic deformation for Model 1 even starts to increase on the condition of P_d = 300 kPa. Therefore, it can be concluded that the higher compaction degree would like to result in convergence for plastic deformation compared with the lower one under the same value of cyclic loading amplitude.

3.2. Vertical Plastic Deformation Under Different Cyclic Loading Amplitude

Since vertical plastic deformation can be quantitatively determined by the deformation curves, the No.1 and No.2 vertical displacement transducers could give two groups of experimental data for the plastic deformation of a given model. Therefore, plastic displacement can be precisely calculated by

averaging the two groups of testing data. The development law of vertical accumulative deformation against loading times is shown in Figure 8. Figure 8a shows the evolutive law of vertical deformation for Model 1 (K = 0.9). When $P_d \leq 100$ kPa, the deformation curves present almost horizontal status when the loading times increase from 80,000 to 100,000. It can be deduced that vertical deformation finally converges towards a constant value, which indicates that plastic displacement tends to be steady under a large amount of cyclic loading times. As P_d increases to 200 kPa or 250 kPa, plastic deformation seems to abidingly develop with the increasing loading times. It can be deduced that the filling model will collapse when loading times are large enough to destroy the filling structure. When P_d = 300 kPa, plastic deformation develops at an overwhelming speed and reaches to 5mm with only 10,000 loading times, and filling structure is broken with relatively fewer loading times. Figure 8b,c show the plastic deformation curves for Model 2 (K = 0.95) and Model 3 (K = 1.0) respectively. Similarly, the deformation curves for the two models firstly converge to some constant value when loading amplitude is relatively low. Then, cumulative deformation is inclined to develop continuously with increasing loading times at relatively higher loading amplitude. Finally, cumulative deformation increases sharply and lead to soil structure broken down instantaneously when amplitude is close to the bearing capacity of the filling model. Obviously, plastic deformation shows quite different developing characteristics under a wide variety of cyclic amplitudes for a given model.

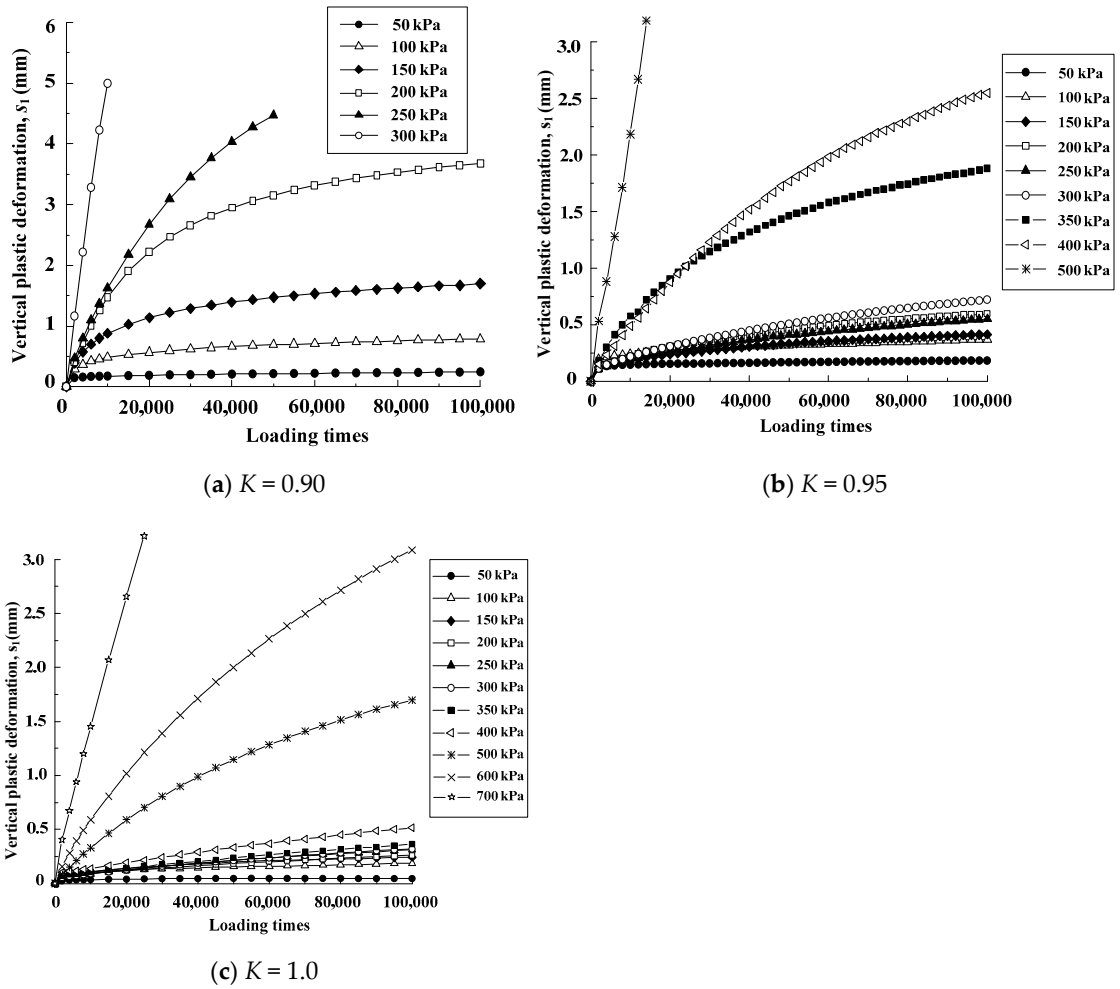

(**a**) K = 0.90

(**b**) K = 0.95

(**c**) K = 1.0

Figure 8. Vertical plastic deformation against loading times for (**a**) Model 1, (**b**) Model 2, and (**c**) Model 3.

The evolutive characteristics of plastic deformation can be further revealed by analyze the deformation rate under cyclic loading. Plastic deformation rate is determined by calculating the

plastic deformation developed every 10,000 loading times. Model 1 with compaction degree of 0.9 is taken as the example to analyze the developing law of plastic deformation rate under cyclic loading. Plastic deformation develops quite rapidly when P_d = 300 kPa. Actually, the deformation rate remains larger than 5 mm per 10,000 loading times at initial loading stage. With loading times increasing, although deformation decreases slightly for a while, it still remains larger than 3 mm per 10,000 loading times. Finally, the filling structure breaks down when cyclic loading reaches to 10,000 times. However, plastic deformation rate seems to decrease gradually with increasing loading times when $P_d \leq 250$ kPa, as shown in Figure 9. Since the deformation rate corresponding to P_d = 300 kPa is so large that it is not plotted in the figure.

Especially, when $P_d < 100$ kPa, evolutive rate of plastic deformation levels off to a small magnitude when loading times reaches to 100,000 times. This phenomenon demonstrates that plastic deformation will finally become steady under low amplitude of cyclic loading. More importantly, deformation rate almost reduces to zero at first 10,000 loading times when P_d = 50 kPa. Therefore, the lower amplitude of cyclic loading, the larger rate of convergence for plastic deformation. On the condition of P_d = 200 kPa and P_d = 250 kPa, plastic deformation develops continuously in spite of the decreasing deformation rate. It is worth noting that the deformation rate finally converges to a constant value, which indicates that plastic deformation seems to develop all the time as long as cyclic loading is applied. Undoubtedly, model structure will break down if plastic deformation develops abidingly.

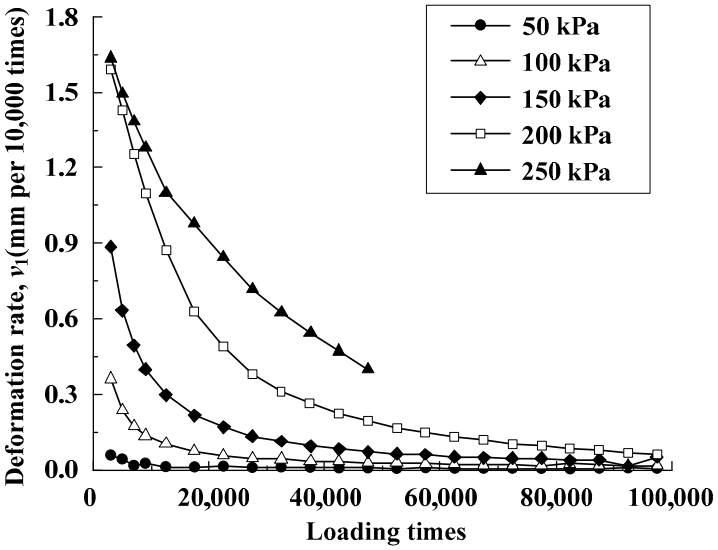

Figure 9. Deformation rate against loading times for Model 1 (K = 0.9).

Although development characteristics of plastic deformation can just be classified into convergency and divergency, apparently, it should be noted that both convergency and divergency could show different evolutive rates at different amplitudes of cyclic loading. When plastic deformation tends to converge towards a certain constant value, lower amplitude would like to result in a higher rate of convergence. However, when plastic deformation is diverging, larger amplitude tends to lead to higher rate of divergence.

3.3. Horizontal Deformation Under Different Amplitudes of Cyclic Loading

The horizontal deformation curve also shows sine pattern under the effect of cyclic loads, which is quite similar to the vertical one. Similarly, plastic deformation can be collected from the horizontal deformation curve to analyze the relationship between accumulative displacement and amplitude of cyclic loading. The horizontal displacement corresponding to the loading times of 100,000 is extracted as the final value for a given amplitude of cyclic loading. Then, accumulative horizontal displacements of these three models are plotted against cyclic amplitude, as shown in Figure 10.

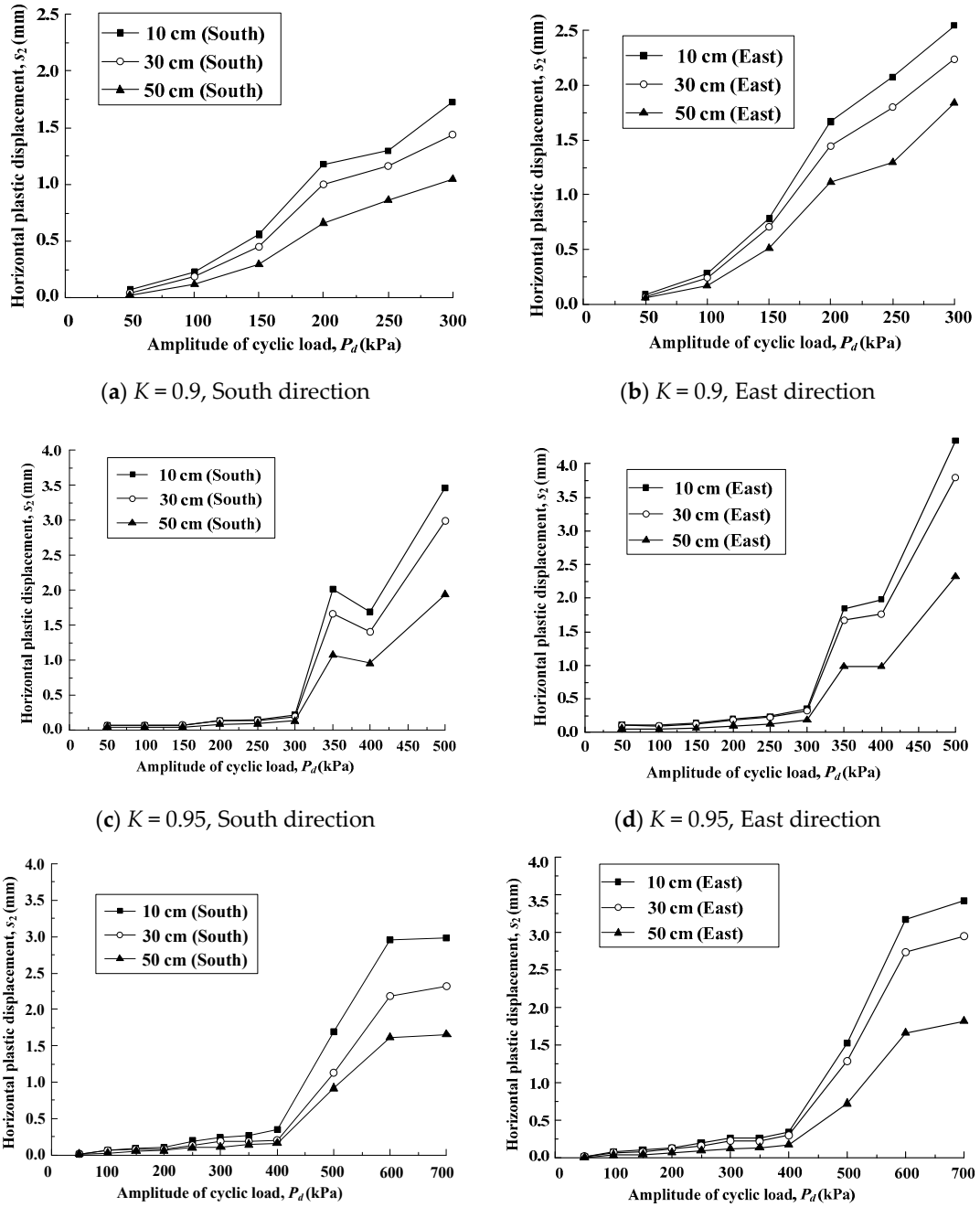

(**a**) K = 0.9, South direction

(**b**) K = 0.9, East direction

(**c**) K = 0.95, South direction

(**d**) K = 0.95, East direction

(**e**) K = 1.0, South direction

(**f**) K = 1.0, East direction

Figure 10. The relationship between horizontal displacement and cyclic amplitude.

Figure 10a,b show the horizontal plastic displacement of Model 1 (K = 0.9) measured by the horizontal transducers distributed on the south brick wall and the east one respectively. Testing data from the transducers on both walls indicate that the model filling with a shallower buried depth would like to have a larger magnitude of horizontal plastic displacement for a given model. Moreover, plastic displacement seems to increase sharply from the amplitude of 150 kPa to 200 kPa for the fillings buried at different depths. It can be deduced that filling structure begins to collapse in this pressure section in all probability, which leads to yielding behavior for the model filling. Moreover, horizontal displacement in the south direction is a bit smaller than that in the east direction, which can be attributed to the differences of boundary conditions provide by the sandbags and the uneven horizontal displacement of the fillings. Although horizontal displacement in the east direction is

slightly larger than that in the south direction, plastic deformations in both directions have quite similar evolutive characteristics.

Figure 10c,d show the horizontal displacement of Model 2 (K = 0.95). The deformation starts to increase overwhelmingly from 300 kPa to 350 kPa. It should be noted that the inflection point of horizontal deformation curve for Model 2 is much more remarkable than that of Model 1. Moreover, the amplitude of cyclic loading corresponding to the inflection point is also significantly larger than the amplitude in Model 1. This illustrates that the filling structure needs a higher level of cyclic loads to arrive at the yielding point when the compaction degree becomes larger. This conclusion can be further verified by the horizontal displacement of Model 3 (K = 1.0), as shown in Figure 10e,f. The inflection points of these horizontal displacement curves locate between 400 kPa and 500 kPa, which is a higher amplitude range compared to 300 kPa–350 kPa. Therefore, the yielding status of model fillings can be reflected by the inflection point on horizontal displacement curve to some extents.

4. Discussion

4.1. Modification for Plastic Deformation Curve

It is described in Boltzmann superposition principle (BSP) that the effects of external loads applied at different moments are linear when they are continued till some later moment [22]. Therefore, effects of different external loads can be added together to evaluate the total results. Hypothesis can be made that plastic strains γ_1(t) and γ_2(t) are produced under the effects of compressive stresses σ_1(t) and σ_2(t) respectively. If σ_1(t) and σ_2(t) are imposed on some model simultaneously, it can be deduced that the strain of γ_1(t) + γ_2(t) will produce according to BSP.

The cyclic loads applied in this study are quite similar to the situation described in BSP. For a given model, 50 kPa of cyclic amplitude is firstly imposed on the model to get the corresponding accumulative deformation. Then, cyclic amplitude increases by another 50 kPa to 100 kPa. Meanwhile, additional plastic deformation can be obtained. However, it should be noted that the additional plastic deformation when P_d = 100 kPa is greatly influenced by the deformation produced at P_d = 50 kPa. By parity of reasoning, the plastic deformation measured under the effect of subsequent loads is significantly lower than the actual value due to the deformation produced previously. In accordance with BSP, accumulative deformation with subsequent loads should be modified by taking the previous plastic deformation into consideration. In detail, the modified plastic deformation can be calculated by the following equations:

$$\boldsymbol{s'}_{\boldsymbol{i}+1} = \boldsymbol{s'}_{\boldsymbol{i}} + \boldsymbol{s}_{\boldsymbol{i}+1} \quad (\boldsymbol{i} = 1, 2, 3, 4 \ldots) \tag{2}$$

$$\boldsymbol{s'}_1 = \boldsymbol{s}_1 \tag{3}$$

where $\boldsymbol{s'}_{\boldsymbol{i}}$ and $\boldsymbol{s'}_{\boldsymbol{i}+1}$ refer to modified accumulative deformations obtained under the effect of the i-th order and (i+1)-th order of cyclic loads respectively, $\boldsymbol{s}_{\boldsymbol{i}+1}$ is plastic deformation produced by the (i+1)-th order of cyclic load. Both $\boldsymbol{s'}_{\boldsymbol{i}}$ and $\boldsymbol{s}_{\boldsymbol{i}}$ are n-dimensional vector quantities composed by n plastic deformations measured at different moments for a given amplitude of cyclic loading. Therefore, these two vector quantities can be expressed as follows:

$$\boldsymbol{s'}_{\boldsymbol{i}}{}^{\mathbf{T}} = \left(s'_{i1}, s'_{i2}, s'_{i3}, s'_{i4}, \ldots\ldots, s'_{in}\right) \tag{4}$$

$$\boldsymbol{s}_{\boldsymbol{i}}{}^{\mathbf{T}} = \left(s_{i1}, s_{i2}, s_{i3}, s_{i4}, \ldots\ldots, s_{in}\right) \tag{5}$$

where s'_{in} refers to the modified deformation at the n-th recorded moment under the effect of the i-th order of cyclic loading, s_{in} is the measured deformation at the n-th recorded moment for the i-th order of cyclic load. It is obvious that the plastic deformation under the first order of cyclic loading is unacted by stress history, so there is no need to modify the measured deformation, as shown by Equation (3).

The modified plastic deformation under different amplitudes of cyclic loading can be precisely calculated by Equation (2), as shown in Figure 11. Model 1 with compaction degree of 0.9 is chosen to demonstrate the developing law of modified plastic deformation. Despite the fact that plastic deformation shown in Figure 11 have quite different magnitudes compared with those in Figure 8a, deformation curves in these two figures have similar tracing pattern. In detail, it can be seen in Figure 11 that plastic deformation tends to converge towards a constant value when P_d = 50 kPa, 100 kPa, and 150 kPa, but shows divergency on the condition of P_d = 200 kPa, 250 kPa, and 300 kPa. Moreover, converging rate becomes smaller and diverging rate becomes larger with amplitude of cyclic loads increasing gradually. With modified plastic deformation determined quantitatively in accordance with BSP, modified deformation rate can be precisely calculated by evaluating the plastic deformation occurred every 10,000 loading times.

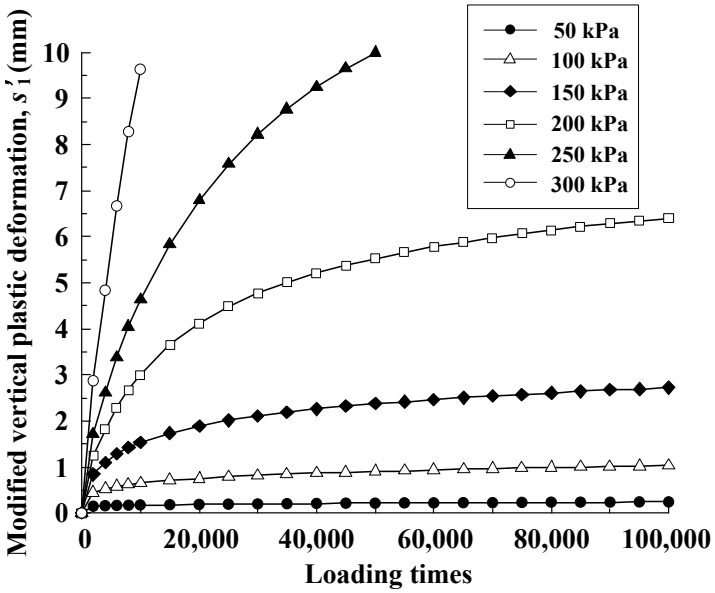

Figure 11. Modified plastic deformation against loading times for Model 1.

4.2. Modified Deformation Rate

Modified deformation rate is quantitatively evaluated on a basis of modified deformation curve for the three models in this study, as shown in Figures 12–14, respectively. Scattered points in the co-ordinates represent modified deformation rates, which are obtained from testing data. It can be seen in Figures 12–14 that plastic deformation rate levels off to a small magnitude rapidly when amplitude of cyclic loading stays at a low level. As cyclic amplitude increases, deformation rate also increases. However, deformation rate also converges as long as the amplitudes remain less than a critical value. Nevertheless, once amplitude rises up beyond the critical value, plastic deformation rate is inclined to keep beyond some constant value in spite of its decreasing trend at initial stage. That is to say, plastic deformation will develop continuously at a constant rate till filling structure breaks down. If the amplitude of cyclic loading increases abidingly, plastic deformation rate starts to increase with loading times, which leads to the model collapse at an overwhelming speed.

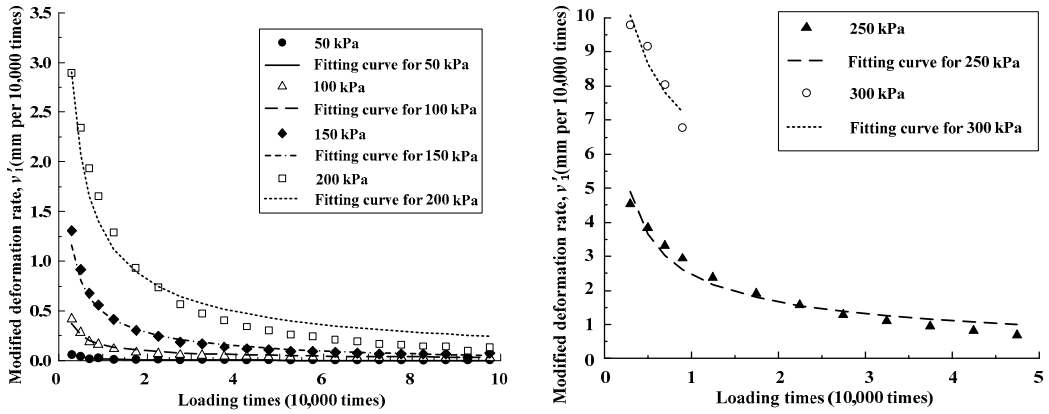

Figure 12. The relationship between modified deformation rate and loading times for Model 1 (K = 0.9) when cyclic amplitude ranges from (**a**) 50 kPa to 200 kPa; (**b**) 250 kPa to 300 kPa.

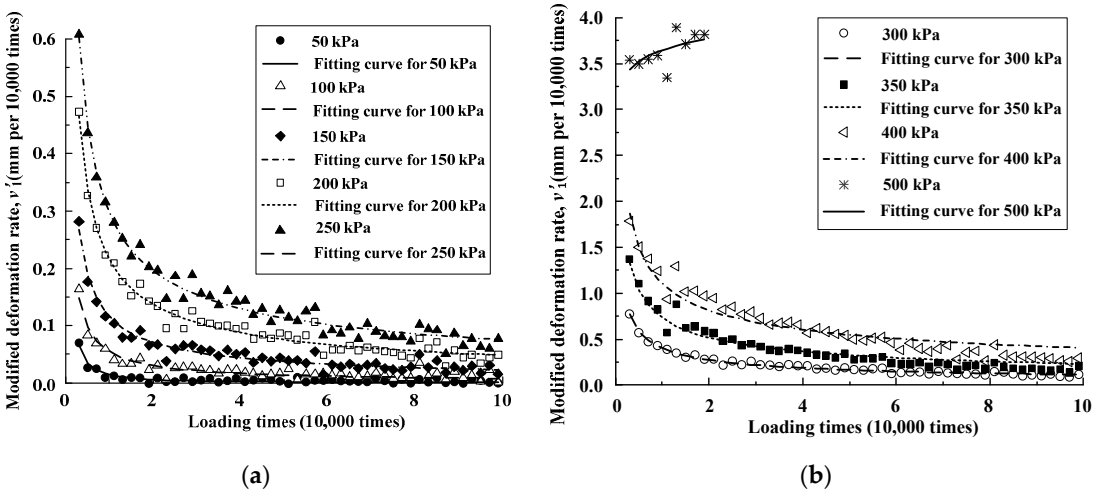

Figure 13. The relationship between modified deformation rate and loading times for Model 2 (K = 0.95) when cyclic amplitude ranges from (**a**) 50 kPa to 250 kPa; (**b**) 300 kPa to 500 kPa.

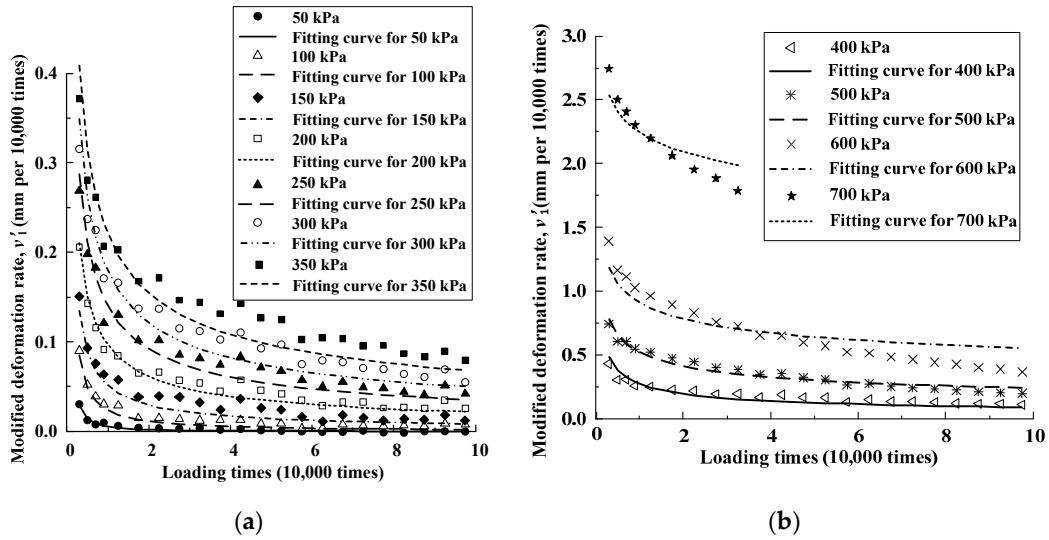

Figure 14. The relationship between modified deformation rate and loading times for Model 3 (K = 1.0) when cyclic amplitude ranges from (**a**) 50 kPa to 350 kPa; (**b**) 400 kPa to 700 kPa.

Following an examination of a great deal of experimental data for both coarse-grained gravels and fine-grained soils, a basic principle is proposed as follows: Under the effect of different amplitudes of cyclic loading, the relationship between accumulative deformation rate and loading times (or elapsed time) can be expressed by a negative power function. This principle implies that plastic behavior of gravel fillings can be expressed by the following equation:

$$v'_1 = CN^{-m} \tag{6}$$

where v'_1 is modified deformation rate, N is loading times, and C and m are constants under a certain amplitude for a given model. The parameter C reflects average deformation rate for a given amplitude of cyclic load. The larger average level of deformation rates at different moments, the higher value of C. The parameter C can be termed as comprehensive evaluation coefficient for plastic deformation rate. Furthermore, the parameter m is an indicator to describe the successional trend for deformation rate curve. Thus, m can be defined as developing tendency coefficient.

Equation (6) can be adopted to describe the modified deformation rate under different amplitudes of cyclic loading for these three models. In the process, the value of the parameters C and m can be determined by regression analysis method, as shown in Table 3. Then, fitting curves can be plotted with modified deformation rate against loading times, as shown in Figures 12–14. All of the fitting curves develop well along the testing data, which indicates that the parameters C and m are reasonably set in the fitting process. Moreover, almost every regression analysis coefficient is higher than 0.90, averaging at 0.919. Obviously, for a given model, there is a group of values for C and m corresponding to a certain amplitude of cyclic loading.

Table 3. The fitting value of C and m for the three models.

P_d (kPa)	K = 0.9		K = 0.95		K = 1.0	
	C	m	C	m	C	m
50	0.017	1.119	0.014	1.287	0.005	1.555
100	0.159	0.708	0.054	0.843	0.023	1.084
150	0.524	0.661	0.115	0.701	0.051	0.804
200	1.348	0.636	0.214	0.646	0.096	0.652
250	2.489	0.550	0.295	0.594	0.139	0.602
300	7.026	0.299	0.400	0.545	0.178	0.559
350			0.730	0.498	0.220	0.515
400			1.104	0.436	0.273	0.481
500			3.647	0.050	0.527	0.394
600					0.910	0.217
700					2.243	0.101

4.3. Comprehensive Rate Evaluation Coefficient C Against Cyclic Amplitude

The comprehensive evaluation coefficient C can be plotted against cyclic loading amplitude, as shown in Figure 15. For a given model with a certain compaction degree, the coefficient C is increased at an accelerated rate with cyclic amplitude P_d increasing. Meanwhile, at a given cyclic amplitude, C is decreased as compaction degree K becomes larger. As mentioned herein before, for the three testing models at different compaction degrees, ground coefficient K_{30} has been evaluated. Furthermore, it has been proposed by Kan [23] that there is an empirical relationship between ground coefficient K_{30} and load bearing capacity P_{cr}, as shown by the following equation:

$$P_{cr} = 2.4K_{30} + 15 \tag{7}$$

Then, bearing capacity P_{cr} for the three testing models can be quantitatively evaluated with Equation (7) as a reference. The values of P_{cr} are 341.4 kPa, 552.6 kPa, and 910.2 kPa for the models with compaction degrees of 0.9, 0.95, and 1.0 respectively. Obviously, there is a positive relationship

between bearing capacity P_{cr} and compaction degree K. Therefore, it can be deduced that coefficient C is negatively correlated with bearing capacity P_{cr} at a given amplitude of cyclic loading.

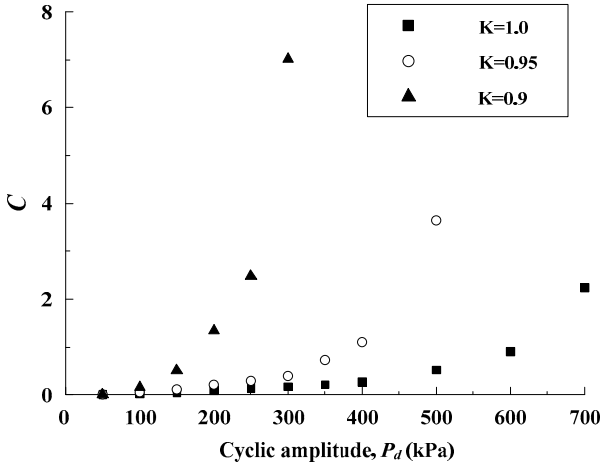

Figure 15. Comprehensive rate evaluation coefficient against cyclic amplitude.

To demonstrate the inner connection between C and P_{cr} as well as cyclic amplitude P_d, comprehensive evaluation coefficient C is further plotted against P_d/P_{cr}, as shown in Figure 16. It is interesting to find that the parameter C under different cyclic loading amplitudes for the three models reasonably develops along a unique curve. As the ratio P_d/P_{cr} increases, the comprehensive evaluation coefficient C also increases exponentially. A regression analysis is performed and gives the following equation a correlation coefficient of 0.85:

$$C = 0.03\left(e^{5.83\frac{P_d}{P_{cr}}} - 1\right) \tag{8}$$

The fitting curve is also plotted in Figure 16. It can be seen that the testing data of the parameter C locates closely along the fitting curve, which demonstrates that Equation (8) can be adopted to evaluate the comprehensive evaluation coefficient C. It is worth recalling that the parameter C is mentioned above as an indicator of average deformation rate for a given amplitude of cyclic loading. Given the expression of Equation (8), it is remarkable that the average deformation rate increases with the amplitudes of cyclic loading, and decreases with bearing capacity P_{cr} as well as compaction degree K increasing. This conclusion is in accordance with our common sense.

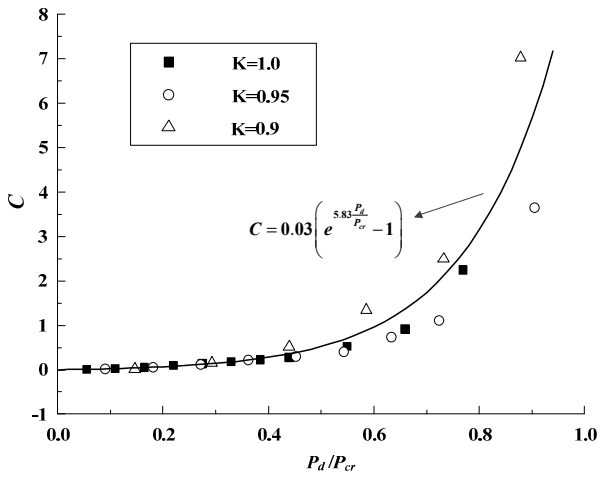

Figure 16. The relationship between C and P_d/P_{cr}.

4.4. Developing Tendency Coefficient m Against Cyclic Amplitudes

Developing tendency coefficient m is a more critical parameter than C to describe the evolving characteristics of plastic deformation. The value of m is plotted against cyclic amplitude level P_d/P_{cr} for the three testing models, as shown in Figure 17. Interestingly, the data points for the parameter m develop along three different sigmoidal curves for the three models. The sigmoidal curves originate from a mutual starting point at the initial stress level. As cyclic amplitude level increases, these three curves disperse from each other gradually. As a consequence, the curves form a unique sigmoidal belt, which can be adopted to demonstrate the evolving characteristics of plastic deformation rate.

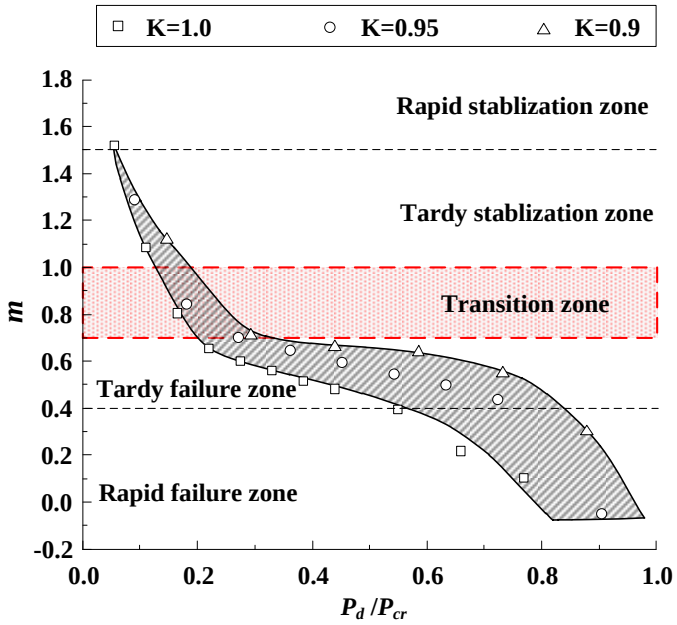

Figure 17. Classification of different evolving states according to the relationship between m and P_d/P_{cr}.

It is worth noting that two inflection points are existed on the sigmoidal belt. One locates approximately at $P_d/P_{cr} = 0.2$ (or $m = 0.7$), and the other corresponds to the condition of $P_d/P_{cr} = 0.6$ (or $m = 0.4$). When $P_d/P_{cr} < 0.2$, the tendency coefficient m decreases remarkably with the increased amplitude level. However, a diminution of decreasing rate for the parameter m occurred when P_d/P_{cr} ranges from 0.2 to 0.6. Finally, as P_d/P_{cr} increase beyond 0.6, m decreases rapidly again, and even reduces below zero. Therefore, the two plastic deformation evolving status corresponding to $P_d/P_{cr} = 0.2$ and $P_d/P_{cr} = 0.6$ respectively are so critical that the evolving characteristics of tendency coefficient m is changed when traverse these two critical values. On the other hand, the relational expression between plastic deformation s'_1 and loading times N can be obtained by carrying out integral operation on Equation (6). The relational expression can be shown as follows:

$$s_1 = \frac{C}{1-m} N^{1-m} + S \tag{9}$$

where S is a constant produced in the integral process. It is obvious that plastic deformation tends to converge towards S with increased loading times when $m < 1$. With overall consideration, $0.7 < m < 1$ can be regarded as the transitional zone of model fillings from stabilization to failure.

With plastic deformation rate evaluated quantitatively, evolving states can be subdivided according to the developing rate of relevant status. In detail, both stabilization and failure status can be subdivided into the rapid and tardy one. It has been mentioned that the first inflection point when $m = 0.7$, together with the data point corresponding to $m = 1$, is the boundary from stabilization to failure. Then, the second inflection point when $m = 0.4$ can be regarded as the boundary of the tardy

failure zone and the rapid one. When $0.4 < m < 0.7$, although plastic deformation is inclined to develop continuously with increased loading times, the decreasing rate of tendency coefficient m is significantly slow. This phenomenon demonstrates that the evolving characteristics of plastic deformation rate just has very slight changes when P_d/P_{cr} ranges from 0.2 to 0.6. Thus, the relevant section can be defined as tardy failure zone. When $m < 0.4$, decreasing rate of the parameter m improves obviously, which indicates that plastic deformation increases at an accelerated speed when P_d/P_{cr} tends to unity. Therefore, this section can be termed as rapid failure zone.

In addition to this, stabilization zone can also be subdivided when $m > 1.0$ in spite of the obvious decreasing trend of the parameter m. A classification criterion can be arbitrarily set that fillings can be judged to fall into rapid stabilization zone on the condition of plastic deformation rate less than 0.001 mm under 30,000 loading times. This is a rigorous standard that only on the condition of P_d = 50 kPa can Model 3 with K = 1.0 fall into rapid stabilization zone. More importantly, the classification criterion corresponds approximately to P_d/P_{cr} = 0.05 (or m = 1.5). In other words, only on the condition of $m > 1.5$ can plastic deformation be limited to 0.001mm with 30,000 loading times. Therefore, m = 1.5 or P_d/P_{cr} = 0.05 can be regarded as the boundary of the rapid stabilization zone and the tardy one.

Finally, it should be noted that horizontal deformation increases sharply at 150~200 kPa, 300~350 kPa, and 400~450 kPa for Model 1, Model 2, and Model 3 respectively. Given the fact that dead load bearing capacity for the three testing models is 341.4 kPa, 552.6 kPa, and 910.2 kPa respectively, the relevant cyclic amplitudes levels P_d/P_{cr} are nearly 0.45~0.55, 0.55~0.65, and 0.45~0.55, which are quite close to the boundary from the tardy failure zone to the rapid one. Obviously, once horizontal deformation starts to increase overwhelmingly, vertical plastic deformation also tends to develop sharply. This indicates that vertical plastic deformation enters into rapid development process and model fillings begin to collapse completely.

A summary can be carried out with the comments mentioned above. When $P_d/P_{cr} < 0.05$ or $m > 1.5$, plastic deformation rate decreases to zero rapidly with just a few of loading times. This status can be judged to locate in rapid stabilization zone. When $0.05 < P_d/P_{cr} < 0.15$ or $1.0 < m < 1.5$, although the decreasing trend of accumulative deformation rate weaken, plastic deformation also finally converges towards a constant value. Undoubtedly, the fillings fall into tardy stabilization zone. The transitional zone corresponds to the condition of $0.15 < P_d/P_{cr} < 0.20$ or $0.7 < m < 1.0$. If P_d/P_{cr} continuously increases from 0.20 to 0.60 and the parameter m decreases from 0.7 to 0.4, plastic deformation tends to develop abidingly, but deformation rate remains at a relatively low level when loading times are large enough. The relevant status can be termed as tardy failure. Finally, as P_d/P_{cr} increases beyond 0.60 and the parameter m decreases below 0.40, not only does accumulative deformation develop continuously, but also the deformation rate stays at a relatively high level from beginning to end. Model fillings can be regarded to fall into rapid failure zone.

4.5. Subgrade Bed Design In Terms of Plastic Deformation

Since subgrade bed is the uppermost structure that directly bears cyclic train load, plastic deformation that occurs at subgrade bed is worthy of sufficient attention in the design process. As mentioned above, the ballasted track has different adaptive capacity for deformation compared with the unballasted one. Therefore, the limitations of plastic deformation should be different for these two types of rail track. Since unballasted track has a more rigorous requirement for plastic deformation, subgrade fillings should be designed to fall into the rapid stabilization zone, i.e., tendency coefficient $m > 1.5$. For ballasted track adopted in high-speed railway, although plastic deformation can be offset by replenishing new railway ballast, the final magnitude of plastic deformation should also be limited to a constant value given the rapid operating trains. Therefore, subgrade bed should fall into the tardy stabilization zone, i.e., $1.0 < m < 1.5$.

However, for ballasted track used in normal-speed railway with relatively fewer traffic volume, maybe subgrade fillings can be designed to fall into the tardy failure zone given the following two

aspects. One is that trains in normal-speed railway operates at a relatively lower speed. The other is that new railway ballast can be added to the ballast bed to offset the plastic deformation for ballasted railway. As revealed in this study, developing tendency coefficient m decreases quite slowly in tardy failure zone, indicating that plastic deformation rate stays nearly steady with the increasing cyclic amplitude. Therefore, subgrade bed for ballasted track in normal-speed railway can be controlled to stay in tardy failure status to save construction cost.

5. Conclusions

A model is constructed with 0.49 m^2 in cross-sectional area and 0.9m in height. The fillings of the model are mainly composed of angular gravels, which are commonly adopted to construct subgrade bed in railway engineering. Cyclic load is applied by the hydraulic-driven loading system to simulate the train load, and deformations of model filling are monitored in real time by eddy current displacement transducers. The conclusions can be drawn from the model test as follows:

(1) Both elastic and plastic deformations are produced in the loading process, while only elastic deformation is recoverable in the unloading process. Thus, plastic deformation is accumulated continuously with the effect of cyclic loading. For a given model with certain compaction degree, the development of plastic deformation is significantly affected by the amplitude of cyclic load. The accumulative deformation tends to converge towards a constant value when cyclic amplitude stays at a relatively low level, and is inclined to develop continuously when the amplitude is high enough to make the filling structure break down.

(2) With the effect of a given level of cyclic amplitude, models with different compaction degree as well as bearing capacity have quite different evolving characteristics of plastic deformation. An appropriate cyclic amplitude may lead to convergence of plastic deformation for a model with a lower compaction degree, but result in divergence of accumulative settlement for another model with a higher compaction degree.

(3) A power function is introduced to investigate the evolving characteristics of plastic deformation rate to subdivide both convergence and divergence status of accumulative deformation. The power function can be expressed as $v'_1 = CN^{-m}$. The comprehensive evaluation coefficient C is an indicator of averaged plastic deformation rate under a given cyclic amplitude. As cyclic amplitude level P_d/P_{cr} increases, the value of C is also exponentially increased. Thus, the parameter C can be evaluated with P_d/P_{cr} known.

(4) The developing tendency coefficient m in the power function is a more critical parameter to describe the evolving characteristics of plastic deformation rate. The value of m shows a sigmoidal curve when plotted against loading times. Subdivision of convergence and divergence status for plastic deformation, which is of great significance to the design of subgrade bed for both ballasted and unballasted railway, can be realized by the analysis of the parameter m.

(5) The evolving characteristics of plastic deformation can be classified into four different patterns in terms of the developing tendency coefficient m. The four patterns are rapid stabilization, tardy stabilization, tardy failure, and rapid failure, with m = 1.5, m = 0.7~1.0, and m = 0.4 as boundaries. It should be noted that the three boundaries are corresponding to the cyclic amplitude level P_d/P_{cr} = 0.05, P_d/P_{cr} = 0.15~0.20, and P_d/P_{cr} = 0.6, respectively. The cyclic amplitude level when horizontal displacement starts to increase sharply is quite close to the boundary of P_d/P_{cr} = 0.6 from tardy failure to rapid failure. Such an amplitude level implies that filling structure completely breaks down.

(6) Since ballasted railway has a better adaptive capacity for deformation compared to the unballasted one, the requirement for limiting value of plastic deformation should be different for these two types of railways. Plastic deformation of subgrade bed in unballasted railway should locate in the rapid stabilization zone, while plastic deformation in ballasted railway should be controlled to fall into the tardy stabilization zone. Such a principle will provide warranty for both economical construction and enduring service for high-speed railway.

Author Contributions: Conceptualization, G.L. and Q.L.; methodology, M.Z. and G.L.; formal analysis, L.G. and M.Z.; investigation, G.L. and H.J.; writing-original manuscript preparation, M.Z. and G.L.; writing-review and editing, M.Z., G.L., Q.L. and H.J.

Funding: This research was funded by National Science Foundation of China, grant number 51408491 and 51878560.

Conflicts of Interest: The authors declare no conflict of interest.

References

1. Railway Technical Research Institute. *Codes for Design of Railway Structure and Some Explanations*; Maruzen Publishing Co. Ltd.: Tokyo, Japan, 2013.
2. National Railway Administration. *Code for Design of High Speed Railway*; China Railway Publishing House: Beijing, China, 2015.
3. Gobel, C.; Lieberenz, K. *Handbook for Soil Structure in Railway Engineering*; China Railway Publishing House: Beijing, China, 2009.
4. Zhang, X.; Zhao, C.; Zhai, W. Importance of load frequency in applying cyclic loads to investigate ballast deformation under high-speed train loads. *Soil Dyn. Earthq. Eng.* **2019**, *120*, 28–38. [CrossRef]
5. Ngo, N.T.; Indraratna, B.; Rujikiatkamjorn, C. Simulation Ballasted Track Behavior: Numerical Treatment and Field Application. *ASCE-Int. J. Geomech.* **2017**, *17*, 04016130. [CrossRef]
6. Dahlberg, T. Some railroad settlement models—A critical review. *Proc. Inst. Mech. Eng. Part F J. Rail Rapid Transit Eng.* **2001**, *215*, 289–300. [CrossRef]
7. Li, D.; Selig, E.T. Cumulative Plastic Deformation for Fine-Grained Subgrade Soils. *J. Geotech. Eng.* **1996**, *122*, 1006–1013. [CrossRef]
8. Lekarp, F.; Dawson, A. Modelling Permanent Deformation Behaviour of Unbound Granular Materials. *Constr. Build. Mater.* **1998**, *12*, 9–18. [CrossRef]
9. Abdelkrim, M.; Bonnet, G.; Buhan, P. A computational procedure for predicting the long term residual settlement of a platform induced by repeated traffic loading. *Comput. Geotech.* **2003**, *30*, 463–476. [CrossRef]
10. Chazallon, C.; Hornych, P.; Mouhoubi, S. Elastoplastic Model for the Long-Term Behavior Modeling of Unbound Granular Materials in Flexible Pavements. *Int. J. Geomech.* **2006**, *6*. [CrossRef]
11. Karg, C.; Francois, S.; Haegeman, W.; Degrande, G. Elasto-plastic long-term behavior of granular soils: Modelling and experimental validation. *Soil Dyn. Earthq. Eng.* **2010**, *30*, 635–646. [CrossRef]
12. Wichtmann, T.; Rondón, H.A.; Niemunis, A.; Triantafyllidis, T.; Lizcano, A. Prediction of Permanent Deformations in Pavements Using a High-Cycle Accumulation Model. *J. Geotech. Geoenviron. Eng.* **2010**, *136*. [CrossRef]
13. Jia, H.Y.; Zhang, D.Y.; Zheng, S.X.; Xie, W.C.; Pandey, M.D. Local site effects on a high-pier railway bridge under tridirectional spatial excitations: Nonstationary stochastic analysis. *Soil Dyn. Earthq. Eng.* **2013**, *52*, 55–69. [CrossRef]
14. Werkmeister, S.; Dawson, A.R.; Wellner, F. Permanent deformation behavior of unbound granular materials and the shakedown concept. In *Transportation Research Record, Journal of Transportation Research Board, No.1757*; Transportation Research Board of the National Academies: Washington, DC, USA, 2001; pp. 5–81.
15. Werkmeister, S. *Permanent Deformation Behavior of Unbound Granular Materials in Pavement Constructions*; Dresden University of Technology: Dresden, Germany, 2003.
16. Werkmeister, S.; Dawson, A.; Wellner, F. Pavement Design Model for Unbound Granular Materials. *J. Transp. Eng.-ASCE* **2004**, *130*, 665–674. [CrossRef]
17. Werkmeister, S. Shakedown analysis of unbound granular materials using accelerated pavement test results from New Zealand's CAPTIF facility. *Pavement Mech. Perform.* **2006**, *154*, 220–228.
18. Heath, D.L. Design of conventional rail track foundation. *Proc. Inst. Civ. Eng.* **1972**, *51*, 49–57. [CrossRef]
19. Cai, Y.; Cao, X.W. Study of the critical dynamic stress and permanent stain of the subgrade-soil under the repeated load. *J. Southwest Jiaotong Univ.* **1996**, *31*, 1–4. (In Chinese)
20. Minassian, G.H. *Behavior of Granular Materials under Cyclic and Repeated Loading*; University of Alaska Fairbanks: Fairbanks, AK, USA, 2003.

21. Hoff, I.; Bakløkk, L.J.; Aurstad, J. Influence of laboratory compaction method on unbound granular materials. In Proceedings of the 6th International Symposium on Pavements Unbound (UNBAR 6), Nottingham, UK, 6–8 July 2004.
22. Kolařík, J.; Pegoretti, A. Proposal of the Boltzmann-like superposition principle for nonlinear tensile creep of thermoplastics. *Polym. Test.* **2008**, *27*, 596–606. [CrossRef]
23. Kan, S.Y. *Heavy Haul Railway Engineering*; China Railway Publishing House: Beijing, China, 2015.